Role of local Ru hexamers in superconductivity of ruthenium phosphide - Supplementary Information -

Robert J. Koch,[1] Niraj Aryal,[1] Oleh Ivashko,[2] Yu Liu,[1,3] Milinda Abeykoon,[4] Eric D. Bauer,[3] Martin v. Zimmermann,[2] Weiguo Yin,[1] Cedomir Petrovic,[1] and Emil S. Bozin[1,*]

[1] *Condensed Matter Physics and Materials Science Division, Brookhaven National Laboratory, Upton, NY 11973, USA*
[2] *Deutsches Elektronen-Synchrotron DESY, Notkestrasse 85, Hamburg, D-22607, Germany*
[3] *Los Alamos National Laboratory, Los Alamos, New Mexico 87545, USA*
[4] *Photon Sciences Division, Brookhaven National Laboratory, Upton, NY 11973, USA*

Note 1: Global structure of metallic state

Sample used in this study exhibits MnP-type *Pnma* structure in its metallic phase above T_1=330 K, Fig. S1, consistent with previous reports [1]. The model yields enlarged U_{22} of Ru 3 times larger than U_{11} and U_{33}, implying quasi-one-dimensional disorder along the *b*-axis in this temperature regime. The origin of this is the formation of hexamer fluctuations discussed in Main Text,

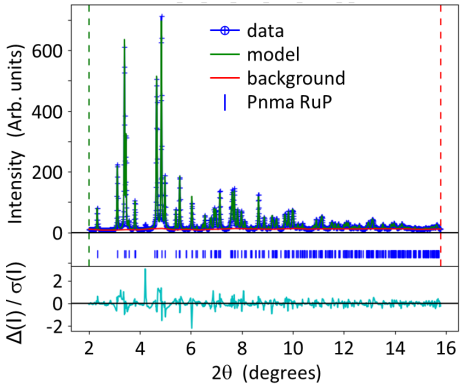

Space group		*Pnma*	R_{wp}=5.4%
a (Å)		5.5257(9)	
b (Å)		3.16306(6)	
c (Å)		6.12725(1)	
Ru	(x, y, z)	(0.9946(2), ¼, 0.2053(4))	
	U_{11} (Å^2)	0.0042(5)	
	U_{22} (Å^2)	0.0168(5)	
	U_{33} (Å^2)	0.0054(3)	
	U_{13} (Å^2)	0.0001(6)	
P	(x, y, z)	(0.19318(2), ¼, 0.5659(4))	
	U_{iso} (Å^2)	0.0067(5)	

FIG. S 1. **Average structure of RuP in metallic regime. (top)** Rietveld fit of the orthorhombic *Pnma* model to 370 K powder data. **(bottom)** Structure parameters extracted from the fit. Small (<5% level by volume) contamination of β-Sn from residual flux is present, evident as a weak reflection at ca. 4.3 degrees 2θ.

* bozin@bnl.gov

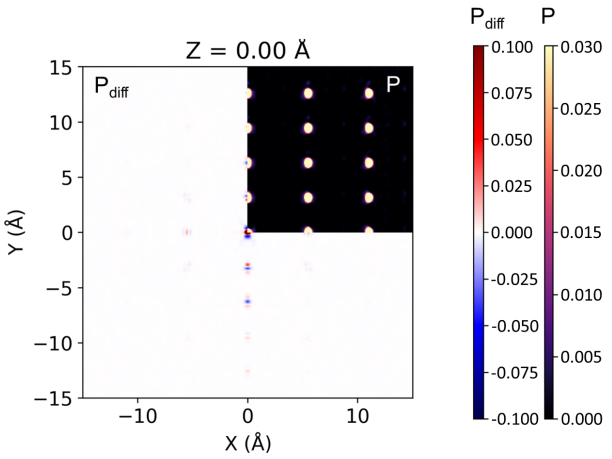

FIG. S 2. **Z=0 slice of RuP 3D-ΔPDF at 350 K.** Highly anisotropic response in differential 3D-ΔPDF; signal decays by 15 Å. Total 3D-PDF is shown in the upper right quadrant.

which are unaccounted for in the *Pnma* model and hence results in observed enlarged Ru ADP components of the principal disorder direction.

Note 2: Local correlations from 3D-ΔPDF

Representative Z=0 slices of 3D-PDF and 3D-ΔPDF are shown in figure Fig. S2. Dominant signal originates from Ru sublattice. As discussed in Main Text, the differential signal is highly anisotropic, reflecting short range structure along the orthorhombic *b*-axis that is different from the global *Pnma* strucure. The extent of local structure correlations is limited to a length-scale of about 15 Å, in agreement with powder derived results.

Note 3: On thermal evolution of RuP lattice

Qualitative assessment of the RuP lattice evolution with temperature is obtained from Rietveld fits of *Pnma* and $P2_1/c$ models to the diffraction data. Although both models are strictly inadequate descriptions of the global structure, *Pnma* below 330 K and $P2_1/c$ over the entire temperature range, they reveal negative thermal expansion (NTE) features of respective (*a*, *b*) and (*a*, *c*) axes in the PG phase, Fig. S3. Similar negative thermal expansion was observed in $CrSe_2$ [2] and attributed to

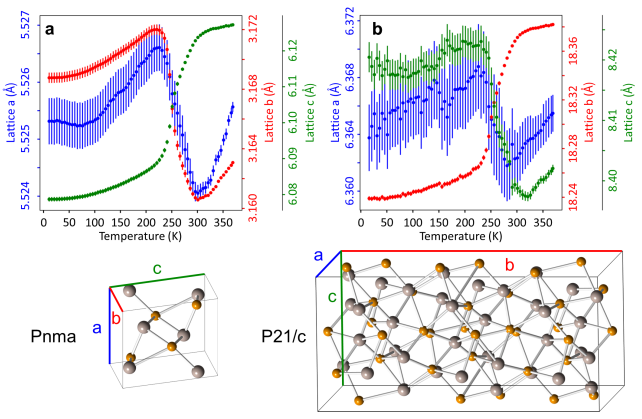

FIG. S 3. **Qualitative T-evolution of the RuP lattice.** **(a)** *Pnma* view from Rietveld refinements. **(b)** $P2_1/c$ view from Rietveld refinements. Bottom panels show structure models with axes color coded to match the colors of the temperature trends shown in **(a)** and **(b)**. Gray spheres represent Ru atoms, while orange spheres mark P.

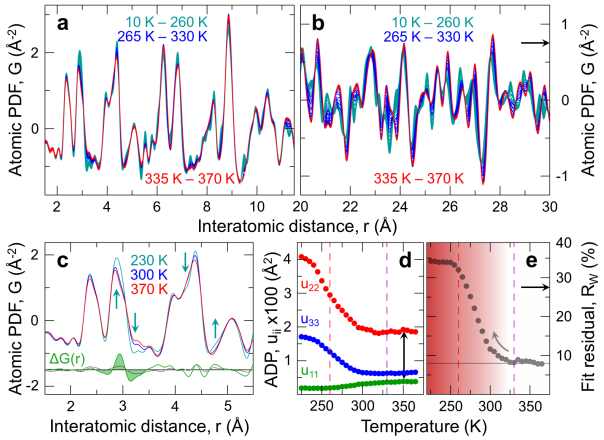

FIG. S 4. **T-evolution of experimental PDFs.** **(a)** Stack of data, collected on cooling, on sub-nanometer length-scale depicting local structure evolution. **(b)** The same stack of data over longer length-scale exhibiting global structure behavior. Distinct temperature ranges corresponding to different phases are color coded, as indicated. **(c)** Comparison of representative PDFs belonging to metallic (red), pseudogap (blue), and nonmagnetic (cyan) regimes, with their differences shown offset for clarity. Corresponding temperatures are as indicated. Arrows mark features addressed in text. **(d)** Evolution of *Pnma* anisotropic ADPs of Ru over a selected temperature range. **(e)** Fit residual for *Pnma* model fit ($15 < r < 50$ Å range) over a selected temperature range. Vertical lines mark transitions observed in diffraction described in Main Text.

fluctuations of metallic clusters. In analogy, we take this NTE as an indicator consistent with complex clustering in the PG regime of RuP. Observed Ru_6 hexamers are presumably the basic building blocks of these clusters.

Note 4: On character of the two transitions

Thermal evolution of experimental PDFs provides useful insights into the character of structural changes at the PG & NM transitions occurring at T_1 and T_2, respectively, on different length-scales. In Fig. S4(a) and (b) we show a stack of data corresponding to the measured temperature range. The data are grouped by color to emphasize the regime they belong to: red (metallic), blue (pseudogap), and cyan (nonmetallic).

Notably, in Fig. S4(b) red PDFs belonging to metallic regime display the sharpest features, with broadening at T_1 and more dramatic redistribution with new peaks appearing below T_2. In the absence of global symmetry changes, PDF features normally broaden on warming accompanied by simultaneous intensity reduction, reflecting enhanced thermal vibrations. Observation of PDF features narrowing and sharpening for $T > T_1$ then indicates global symmetry increase (*Pnma*) as the long range hexamer order is removed, or, conversely, broadening for $T < T_1$ and redistribution for $T < T_2$ with new PDF peaks occurring in the NM phase signifies global symmetry reductions at both transitions. In contrast, features describing the very short range structure, Fig. S4(a), exhibit canonical thermal behavior where the features gradually sharpen on cooling across T_1, and more abrupt changes across T_2.

In Fig. S4(c) three experimental PDFs representative of three temperature regimes are shown over a narrow r-range, with their differences underneath. The change between 370 K and 300 K (bracing T_1, data are 70 K apart) is small and thermal in character, with no evidence of change in the local symmetry. On the other hand, the change between 300 K and 230 K (bracing T_2, data are 70 K apart) is substantial. In addition to sharpening that is expected on cooling, the change involves dramatic intensity redistribution involving distinct features around ca. 3 Å which are consistent with hexamer stabilization and further local distortions in the NM phase, as discussed in Main Text. While the symmetry of the global structure changes at both transitions, lack of local structure change across T_1 implies an order-disorder component of the PG transition where at least partial ordering of hexamers is established, with local symmetry changing only across T_2 and in the NM phase and consistent with further complex oligomerization discussed in Main Text. Evolution of anisotropic ADPs of Ru and the *Pnma* fit residual, Fig. S4(d), (e), support this picture.

Note 5: Single crystal diffraction considerations

Selected reciprocal space slices of single crystal diffraction data are shown in Fig. S5. In the metallic phase at 350 K pronounced arcs (Fig. S5(a)), and butterfly & oval features (Fig. S5(b)) can be seen, constituting a rich diffuse scattering signal associated with short range hexamer precursors discussed in Main Text. In the pseudogap phase at 300 K superlattice reflections appear (Fig. S5(c), (d)), while the diffuse scattering signal evolves. In the nonmagnetic phase at 10 K new superlattice re-

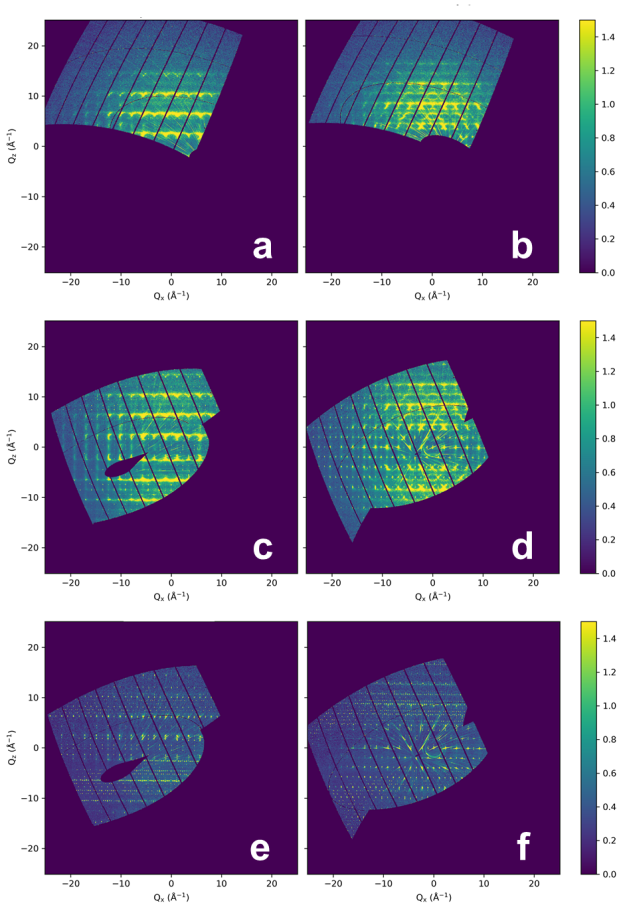

FIG. S 5. **Crystal diffuse scattering: broad Q-range.** Selected slices of reciprocal space data: Q_y=5.97 Å^{-1} (left) and Q_y=2.20 Å^{-1} (right) at 350 K, (a) and (b), 300 K, (c) and (d), and 10 K, (e) and (f).

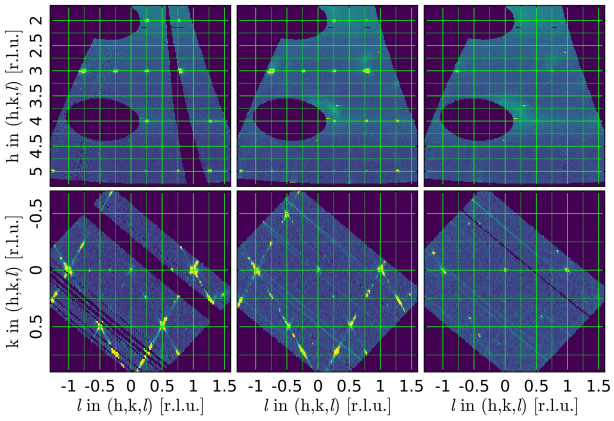

FIG. S 6. **Bragg scattering scan around (200)$_{HT}$.** Top row of panels is k=1/4 slice at 222 K (left), 270 K (middle) and 343 K (right). Bottom row of panels is h = 20/4 slice at 222 K (left), 270 K (middle) and 343 K (right).

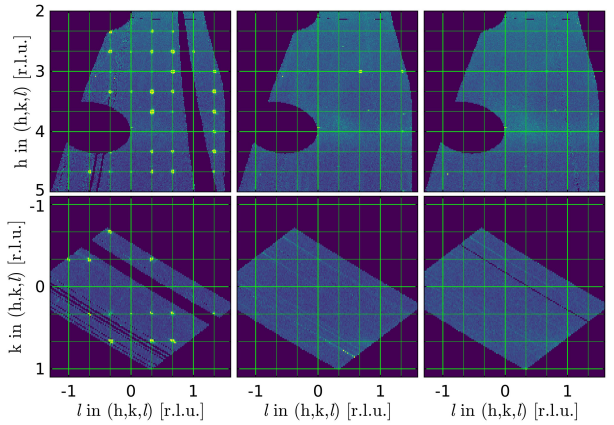

FIG. S 7. **Bragg scattering scan around (200)$_{HT}$.** Top row of panels is k=1/3 slice at 222 K (left), 270 K (middle) and 343 K (right). Bottom row of panels is h = 14/3 slice at 222 K (left), 270 K (middle) and 343 K (right).

flections are observed, with no apparent diffuse signal observable (Fig. S5(e), (f)).

Additional single crystal scattering data collected on cooling over a narrower portion of reciprocal space around (200)$_{HT}$ reflection in *Pnma* notation show appearance of different superlattice reflections, similar to these from the original report [1]. Below T_1, in the PG phase, 1/4 and 1/5 superlattice reflections are observed (Fig. S6) and persist down to the lowest measured temperature. They coexist with 1/3 peaks associated with the NM phase, addressed next, that appear below T_2, as can be observed at the lower left panel of Fig. S6. The spurious peaks observed at high temperature result from crystal twinning and are still present along new superstructure peaks in the PG phase. In addition, a strong diagonal diffuse scattering is also present.

Below T_2, 1/3 reflections appear in all three directions, Fig. S7. The two peaks for h = 3 and l very close to 2/3 and 4/3, are not related to these superstructure peaks, but are most probably derived from the diffuse scattering at observed at integer h values. The diffuse scattering observed in metallic and pseudogap regimes would suggest that it is a precursor for the NM structural transition. However, more likely scenario is that the ordering of hexamers *d*oes not complete by the time temperature at which non-magnetic phase sets in is reached. The preference for the latter interpretation stems from the observation of diffuse scattering appearing in relation to 1/4 rather than 1/3 reflections. This supports scenario discussed in Main Text, according to which hexamer fluctuations are precursors to pseudogap phase, which order at the T_1 transition. Observation of 1/3 reflections below the T_2 transition is fully consistent with dimerization observed in the local structure model along the orthorhombic *a*-axis, as well as further complex oligomerization of hexamers reflecting stripe-like lamellar ordering details of which require full crystallographic structure solution. We note here that the observed superlattice peaks occur slightly off of their nominal positions, which could imply that the underlying structure is incommensurate. In

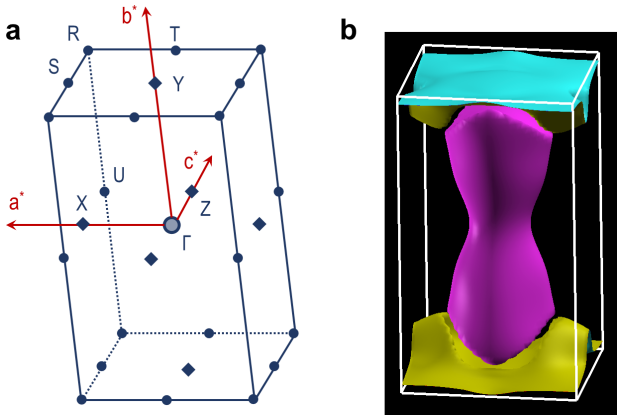

FIG. S 8. **Reciprocal space details.** (a) The Brillouin zone of the orthorhombic cell showing reciprocal lattice vectors and high symmetry points. (b) Calculated Fermi surface corresponding to the orthorhombic *Pnma* phase.

this case locally commensurate structure domains separated by discommensuration domain walls is a distinct scenario. Notably, the length-scale probed by the powder PDF is sufficiently small as to represent the intra-domain structure.

Note 6: Reciprocal space details

The directions discussed in Main Text that connect high symmetry points in the Brillouin zone of the orthorhombic *Pnma* structure are shown in Fig. S8(a). Notably, calculated Fermi surface for the global structure at 370 K features flat sheets at the Brillouin zone edge, whose normal vector is parallel to the b* axis of the reciprocal space, as seen in Fig. S8(b).

[1] Hirai, D., Takayama, T., Hashizume, D. & Takagi, H. Metal-insulator transition and superconductivity induced by Rh doping in the binary pnictides Ru*Pn* (*Pn* = P, As, Sb). *Phys. Rev. B* **85**, 140509 (2012). URL `https://link.aps.org/doi/10.1103/PhysRevB.85.140509`.

[2] van Bruggen, C. F., Haange, R. J., Wiegers, G. A. & de Boer, D. K. G. $CrSe_2$, a new layered dichalcogenide. *Physica B+C* **99**, 166 (1980). URL `https://www.sciencedirect.com/science/article/pii/0378436380902260`.